The Making of a Surface Current Atlas of the St. Lawrence Estuary, Canada

F. J. Saucier, J. Chassé, M. Couture, R. Dorais, A. D'Astous, D. Lefaivre, A. Gosselin
Maurice Lamontagne Institute, Department of Fisheries and Oceans
850, Route de la Mer, Mont-Joli, Quebec, Canada G5H 3Z4
Email: saucierf@dfo-mpo.gc.ca

Abstract

A 3D numerical model for water levels, currents, density, and turbulent quantities is applied to the St. Lawrence Estuary under typical summer conditions. The lateral resolution is 400 m with 20 layers in the vertical. The model results were compared to 51 current-meter records, showing 15% average relative error. The simulations reproduce the strong large-scale baroclinic motions forced by the action of tides on the density field. Month-long simulations were synthesized into 108 surface current charts for nine regions of the Estuary and over 12 hourly periods through a semi-diurnal tidal cycle. Linear correction factors were derived to take into account the diurnal to fortnightly irregularities of the tide. These charts make up the new Atlas of tidal currents published by the Canadian Hydrographic Service.[1] The map scales were chosen to display Lagrangian currents. The errors made when using the new Atlas were estimated by comparing its current predictions with over two thousand 20 minute-long, Global Positioning System surface drifts acquired over all tidal phases and regions of the Estuary, showing differences of less than 0.7 m s^{-1} and 15° in current magnitude and direction, respectively, at the 90% confidence level.

1 Introduction

Late Holocene glacial events forged the present shape of the Estuary and Gulf of St. Lawrence. The main feature is the major glacial valley called the Laurentian Trough, which extends 1500 km from the continental margin to an abrupt end near the city of Tadoussac (Fig. 1). The Upper Estuary, about 180 km long and

extending to Québec City, has many fjord-like features, such as relatively deep basins separated by shallow underwater sills and banks. Its waters are stabile stratified and made of a partial mixture of freshwater from the St. Lawrence River (mean flow of 1.1 x 10^4 m^3 s^{-1}) and denser intermediate waters moving in below from the Gulf of St. Lawrence, e.g. Neu.[2] The Saguenay Fjord, with an average freshwater outflow of 1.3 x 10^3 m^3 s^{-1}, and other smaller tributaries enhance estuarine circulation near the outer sills. Mixed, predominantly M_2 tides propagate from the Atlantic Ocean and range from 4.4 m in the Lower Estuary to over 7 m at Île d'Orléans. They produce topographically and gravitationally controlled complex 3D currents over 2 m s^{-1} throughout. The tides dissipate through bottom friction, mixing, and internal wave generation in the Upper Estuary and dissipate further with bottom friction until they vanish about 150 km upstream from Québec City.

The strong current and inclement weather of the St. Lawrence cost lives and represent a permanent hazard to navigation. The objective of this paper is to document the steps taken to produce charts of surface tidal currents for the St. Lawrence Estuary, under typical summer conditions, that can form a reference document for navigators and other users. To achieve this goal, we make use of a 3D numerical model for water levels, currents, and density changes. We compare the results with historical current-meter records as well as new observations of surface currents acquired with surface drifters.

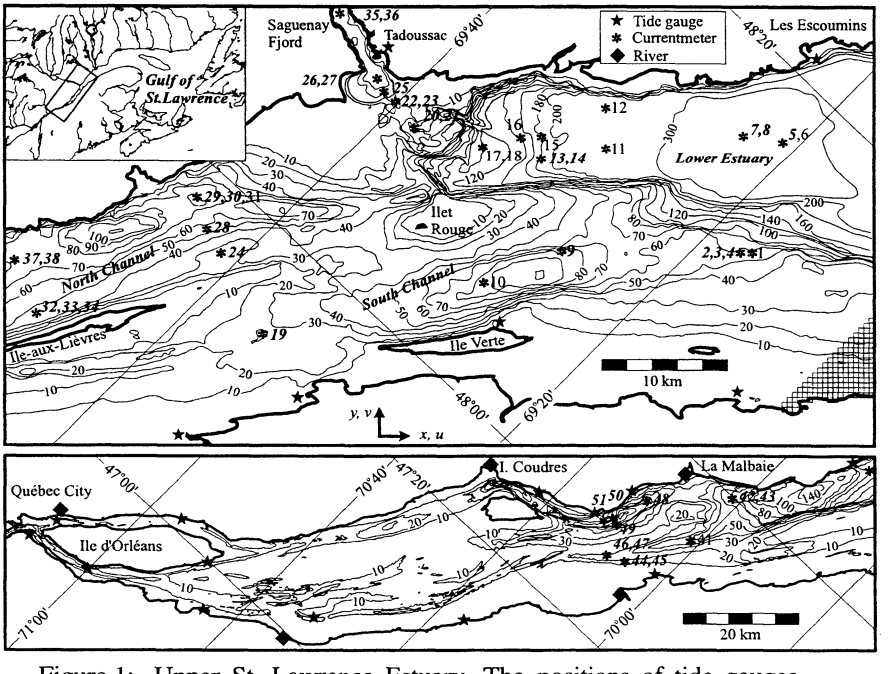

Figure 1: Upper St. Lawrence Estuary. The positions of tide gauges, main tributaries, and historical current meters are shown. A subarea of the grid is shown. The boxed area in the upper left shows the model domain. The depths are in meters.

2 Numerical Modeling

A hydrostatic solution to the mass, momentum, and density conservation in the Boussinesq approximation is reached from the finite difference formulation initially put forward to model oceanographic processes by Backhaus.[3] This model was thereafter modified by Stronach & al.[4] and Saucier & Chassé.[5]

2.1 Governing Equations

Mass conservation:

$$\frac{\partial u}{\partial x}+\frac{\partial v}{\partial y}+\frac{\partial w}{\partial z}=0 \tag{1}$$

Momentum conservation:

$$\frac{\partial u}{\partial t}+\mathbf{u}\cdot\nabla_H u-fv+\frac{1}{\rho}\frac{\partial P}{\partial x}-\frac{\partial}{\partial x}\left(A_H\frac{\partial u}{\partial x}\right)-\frac{\partial}{\partial y}\left(A_H\frac{\partial u}{\partial y}\right)-\frac{\partial}{\partial z}\left(A_{VM}\frac{\partial u}{\partial z}\right)=0 \tag{2}$$

$$\frac{\partial v}{\partial t}+\mathbf{u}\cdot\nabla_H v+fu+\frac{1}{\rho}\frac{\partial P}{\partial y}-\frac{\partial}{\partial x}\left(A_H\frac{\partial v}{\partial x}\right)-\frac{\partial}{\partial y}\left(A_H\frac{\partial v}{\partial y}\right)-\frac{\partial}{\partial z}\left(A_{VM}\frac{\partial v}{\partial z}\right)=0 \tag{3}$$

Density conservation:

$$\frac{\partial \sigma_t}{\partial t}+\mathbf{u}\cdot\nabla\sigma_t-\frac{\partial}{\partial x}\left(A_H\frac{\partial \sigma_t}{\partial x}\right)-\frac{\partial}{\partial y}\left(A_H\frac{\partial \sigma_t}{\partial y}\right)-\frac{\partial}{\partial z}\left(A_{V\sigma}\frac{\partial \sigma_t}{\partial z}\right)=0 \tag{4}$$

Hydrostatic equation:

$$\frac{\partial P}{\partial z}=-\rho g \tag{5}$$

with $\rho = \rho_0 + \sigma_t$. The velocity is $\mathbf{u} = (u,v,w)$ along the horizontal axes x and y (see Fig. 1) and vertical axis z (positive upward), f is the Coriolis parameter, P is the pressure, ρ is the density, ρ_0 is the reference density, σ_t is sigma-t, A_H is the horizontal eddy diffusivity for momentum and density, g is the gravitational acceleration, and A_{VM}, $A_{V\sigma}$ are the vertical eddy viscosity and diffusivity, respectively.

As in Backhaus[3], both the external and internal modes are treated implicitly and no major restriction on the time step occurs other than for the accuracy in amplitude and phase of gravity waves. The horizontal diffusivities are as described in Smagorinsky[5,6]. We follow Mellor & Yamada[7] in the implementation of a level 2 turbulence closure model. Since no general formulation exists for specifying the turbulent length scale (see Davies & al.[8] for a review) and the data are inadequate to suggest better approximations, we extract a basic scale from an integral of the turbulence energy, e.g. Mellor & Durbin.[9]

2.2 Boundary Conditions and Experimental Setup

The model domain extends from Rimouski to the upper limits of tidal influence

near Trois-Rivières and at the head of the Saguenay Fjord (boxed region in Fig. 1). The grid resolution is 400 m in the horizontal and the vertical coordinate is described by 20 model layers (based at depths of 5, 10, 15, 20, 25, 30, 35, 45, 55, 65, 75, 90, 105, 125, 150, 175, 200, 250, 300, and 350 m). The hydrographic soundings and the mean sea level (Z_0) (added to charted depths) were interpolated on this grid. The depth of the bottom layer is locally corrected to the observed depth in the momentum and density equations.

The hydraulic heads of the St. Lawrence Estuary and Saguenay Fjord, interpolated from geodetic leveling at tide gauge stations, were added to the barotropic pressure gradient. Twenty other tributaries with significant flow rates (greater than 10^2 m^3 s^{-1}) were specified as boundary conditions in the momentum and density equations. The amplitude and phase of the 15 main water level tidal constituents are specified along the open boundary in the Lower Estuary. We use the tide gauge observations at the eastern grid corner (Rimouski), and, to describe the changes in the constituents along the open boundary, we make use of another implementation of the model described herein for the Gulf of St. Lawrence that was forced at the mouth from the observed water level constituents (not shown).

The flow normal to any solid boundary is set to zero. A free-slip boundary condition is applied to the side walls, those generally bounding shallow (i.e., 5 m) layers at the given grid resolution. The bottom stress is a quadratic function of bottom velocity of the Manning-Chezy type.[10] The initial density condition is specified from observed summer density profiles acquired in 1975 in the Upper Estuary and the mean summer profile from Forrester[11] in the Lower Estuary. During inflow, a zero gradient condition is applied to all velocity components on the eastern open boundary and density is specified from the mean summer profile derived as the initial condition there. During outflow ($u > 0$), the radiation condition

$$\frac{\partial \xi}{\partial t} + u\frac{\partial \xi}{\partial x} = 0 \tag{6}$$

is specified to $\xi = u, v$, while zero gradient is specified for density.

The model spins up from rest and the boundary forcing ramps up for two days. Density, mixing, and circulation approach a near steady state, modulated by tides, within one week, representing the approximate residence time of freshwater in the Upper Estuary. The analyses below are based on the results from the last 30 days of a 40 day simulation in this context.

3 Model Calibration and Validation

The calibration was performed by adjusting bottom friction over a few simulations to reproduce water level tidal harmonic amplitudes and phases over the model domain (derived from data and model results following Foreman[12]). The relative error of the water level tidal harmonic constituent range from 5 to 10% in amplitude and is less than 5° on the average for constituents M_2, S_2, N_2, K_1, O_1 (with respective average amplitudes of 1.7 m, 0.5 m, 0.3 m, 0.3 m, and 0.2 m). Fig. 2 shows the modeled M_2 phase and amplitude downstream from Québec.

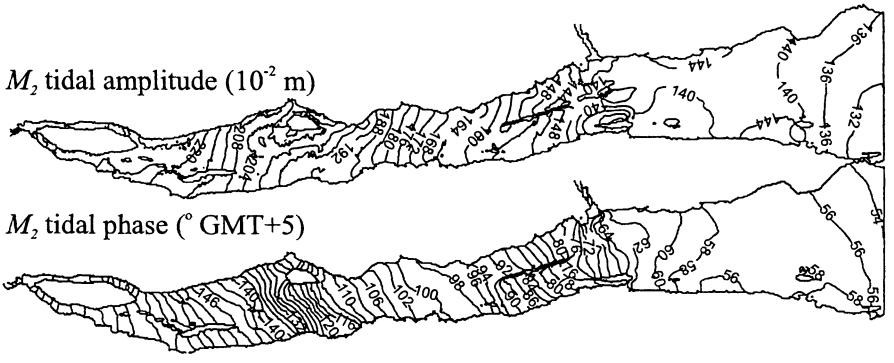

Figure 2: Modeled co-amplitude and co-phase lines for the M_2 tide.

After calibration for water levels, the model results were compared with 51 current-meter records, each ranging from a few days to one summer in length, acquired between 1973 and 1982. Fig. 3 shows the observed hourly u current component (see axes on Fig. 1) against the predictions issued from model-derived tidal constituents. The mean error of the hourly velocity u and v components is 0.25 m s^{-1}, or 15% relative error. As seen in Fig. 3, meteorological events are not significant in the current records. Large tidal current variations take place both in the horizontal, as controlled by the topography, and in the vertical, as controlled by the stratification.

4 Currents, Density Effects, and Synthesis of the Atlas

The irregularities in the mixed tides mainly affect the magnitude of the modeled semi-diurnal changes in the circulation and density fields. Qualitatively, we see small differences from one semi-diurnal cycle to the next. This leads to the basic assumptions used to synthesize the Atlas: (1) only the magnitude of the tidal current is affected by irregularities in the amplitude of the semi-diurnal oscillation, (2) linear corrections may be applied to the current magnitude given the tidal predictions for water level at the reference ports[13], and (3) the time scale is made with origins at high or low waters, and a time correction may normalize the actual length of the tidal cycle to the average length of 12.42 hours. Clearly, such assumptions weaken the power of the full simulation but provide a practical solution. The resulting errors are examined from independent surface current measurements below.

From the month-long solution, we extract the surface layer currents for a semi-diurnal tidal cycle of average period (12.42 hrs) and range (2.5 m) at the reference port of Pointe-au-Père (located near the open boundary). To display the tidal currents, we decompose the tidal period into 12 one-hour segments plus two gaps having an average length of 0.21 hrs. Fig. 4 shows four of the 108 surface current charts that comprise the Altas[1]. The spatial and temporal scales of the deformation in the Upper Estuary are such that it is appropriate to display Lagrangian currents.

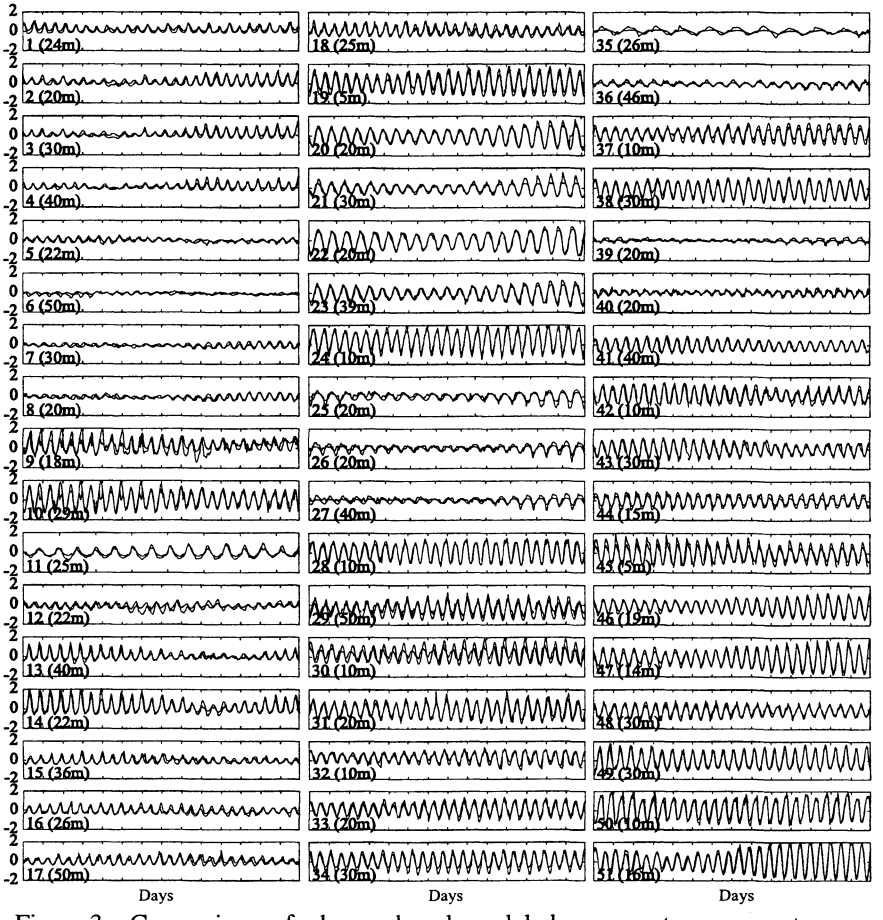

Figure 3: Comparison of observed and modeled u current component (along the axis of the Estuary), in m s^{-1}, at the positions shown in Fig. 1 (two full lines per panel). The tidal harmonic synthesis of the modeled velocity is compared with hourly unfiltered observations. The depth of each instrument is shown in parentheses. The horizontal time axis spans the record length to a maximum of 14 days, but actual records may be longer.

These add to the Eulerian representation in that the charts directly indicate the trajectory of surface tracers (e.g., a hypothetical oil spill or a person overboard). Lagrangian currents were computed by deploying a surface tracer at each grid point and using a fourth order Runge-Kutta velocity integration with the model time step of 60 sec.

Tidal currents are highly baroclinic seaward of Île-aux-Coudres. Surface density effects are best illustrated in Fig. 5 (for the region displayed in the upper

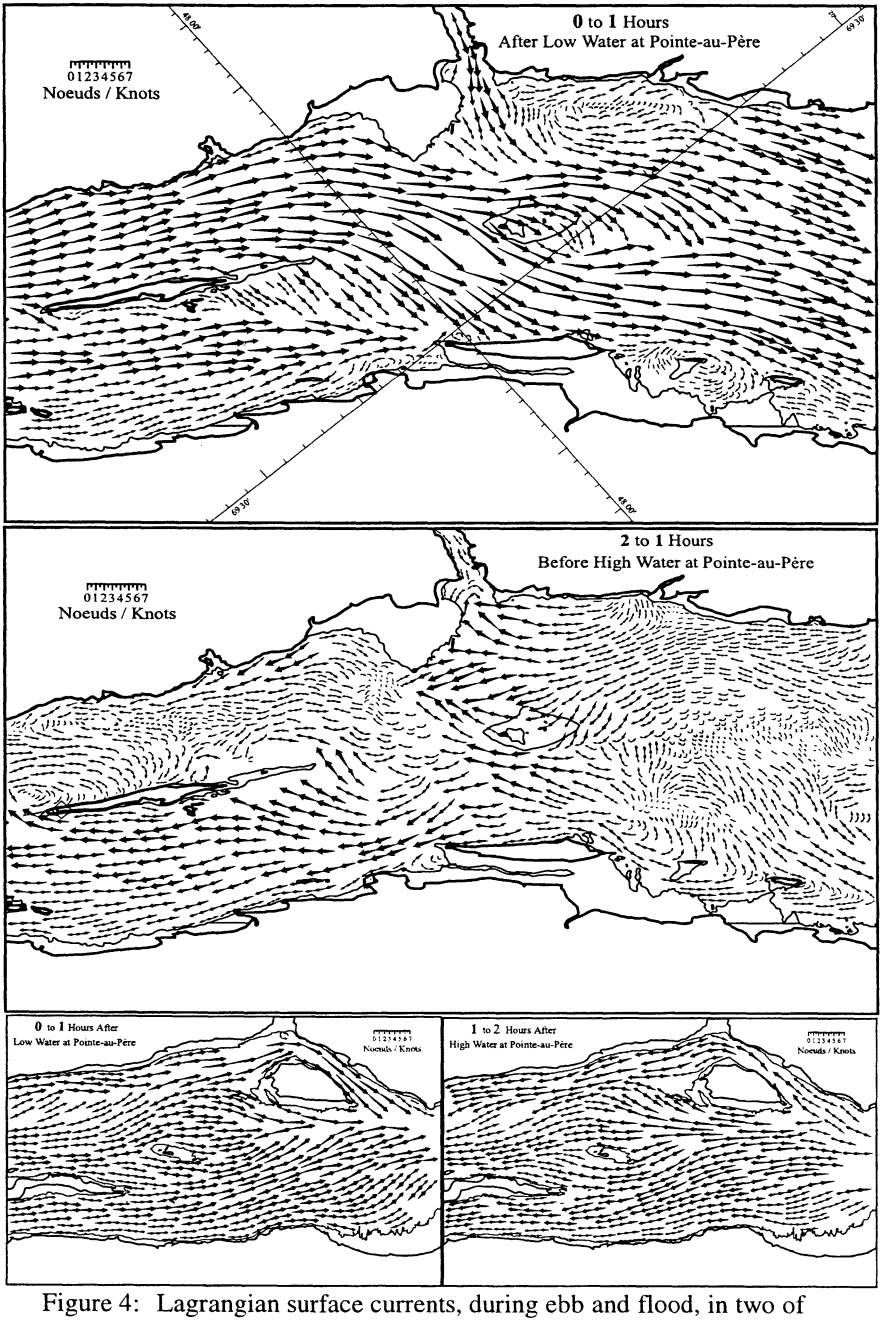

Figure 4: Lagrangian surface currents, during ebb and flood, in two of the nine regions as they appear in the Atlas. Each vector triplet represents the current and the trajectory of surface water over one hour through segments of 20 minutes.

surface jet from the North Channel, with velocities exceeding 3 m s^{-1} during spring tides, that branches around Ilet Rouge. The northern branch is intensified by the Saguenay waters and meets with the southern branch on the southeastern bank of the Lower Estuary. There, as observed[14] and modeled, the flow only reverses with large flood tides.

At the onset of the flood, the surface waters from the Lower Estuary move southeasterly from the head of the Laurentian Trough. The ebb-flowing surface jet slows down and is deviated southward against the emerging dense waters. Shortly after low water, intermediate waters are pushed up toward the surface along the North Shore of the Lower Estuary against the outflowing Saguenay surface waters. About two to three hours after low water, a segment of this frontal structure rotates clockwise at the mouth of the Saguenay Fjord (see Fig. 5) until the dense waters find the paths over the sill (20 m depth) and into the outer Fjord basin. Convergence then begins along the front. An hour later, the dense waters reach the outer Estuary sill just west of Ilet Rouge (35 m depth) and, in turn, initiate subduction into the North Channel. The converging fronts intensify and maintain stationary positions over the lee sides of the sills until high water. Intermediate waters originating from below 75 m depth move to the surface within three hours. The surface fronts are associated with internal hydraulic jumps.[15,5] The dense waters passing the sills set up gravity currents on the landward slopes. The surface waters of the St. Lawrence and the Saguenay stop their seaward displacement and remain nearly stationary close to Île-aux-Lièvres and in the Saguenay Fjord, only slowly backing up during large flood tides (e.g., second panel in Fig. 4). In the two hours after high water, upwelling stops on the outer slopes while bottom density currents are still strong over the inner slopes. In the period between two and five hours after high water, surface waters drain to re-stratify the head region.

For each current chart and 55 tidal cycles from the simulation, we extracted the relationship between the ratio of current intensity over charted current and the tidal range (water level difference between the two bounding extremes at the port of reference). Fig. 6 shows two such relationships for a period of full ebb flow and one of slack waters in the second region displayed in Fig. 4. For each data set, we seek a linear model to explain the variations in the current magnitude. This model is then

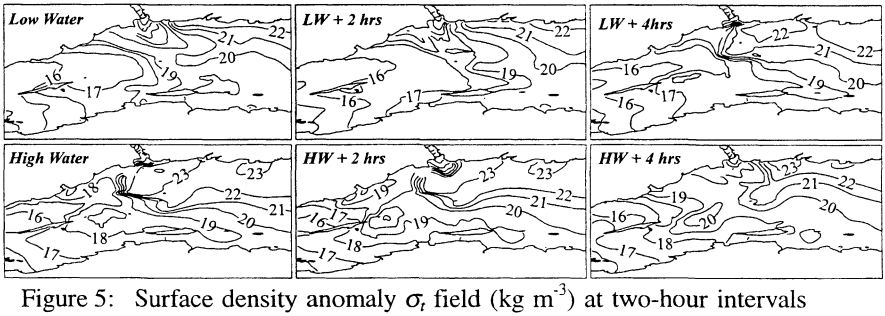

Figure 5: Surface density anomaly σ_t field (kg m^{-3}) at two-hour intervals over a mean semidiurnal cycle between Les Escoumins and Saint-Siméon (region shown in the top panels of Figs. 1 and 4).

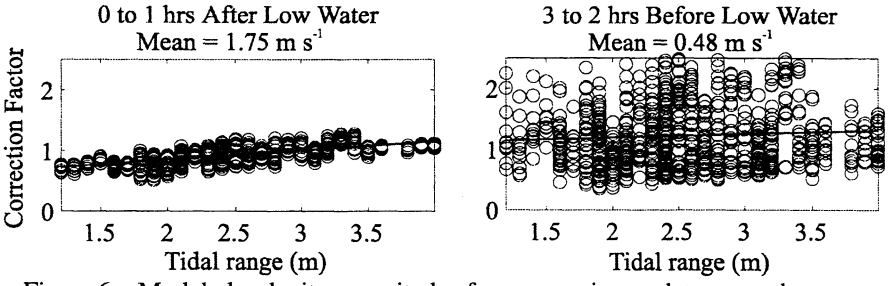

Figure 6: Modeled velocity magnitude, for one region and two one-hour time periods, as a function of tidal range normalized by the velocity solution for a mean tidal range at Pointe-au-Père (2.5 m).

displayed on each chart so that the user can correct the currents from the published tidal height predictions. The predictive power of this model is relatively good during ebb and flood and is highest in the barotropic regime of the upstream regions.

5 Validation of the Atlas

The error analysis must account for the approximations used to synthesize the model information. We therefore deployed over 600 Global Positioning System surface drifters through all regions and phases of the tides during the summers of 1994 and 1995 for one-half to two hours each. We compared their trajectories with the predictions made from the current charts and the associated correction factors.

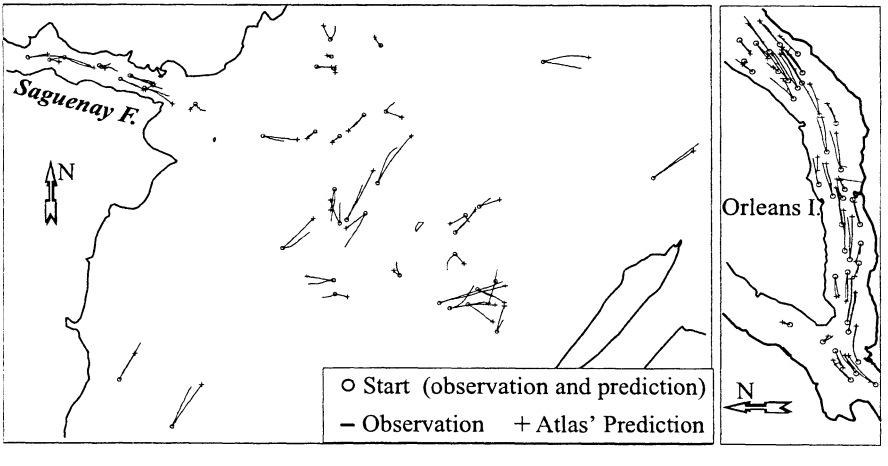

Figure 7: Sample of comparisons between observed 20-minute drifter trajectories and the predicted trajectories from the current synthesis, including the linear correction on current magnitude.

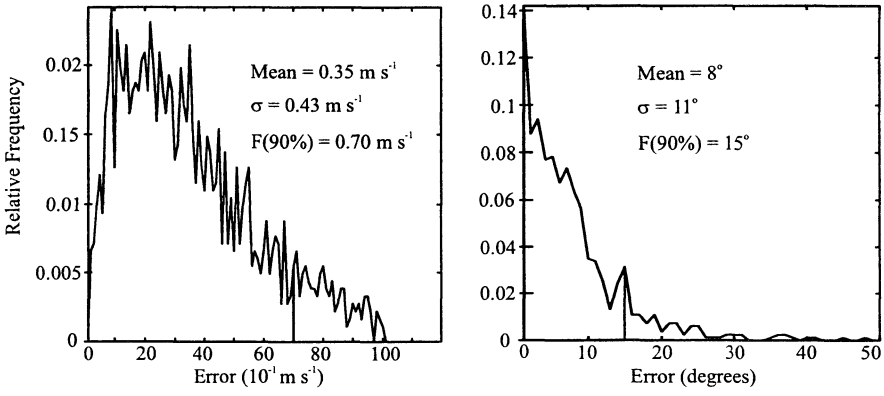

Figure 8: Distribution of 2100 comparisons between the current predictions from the Atlas and the surface trajectories in velocity magnitude (left) and direction (right, for current > 0.7 m s^{-1}). The vertical bar indicates the 90% confidence level.

Fig. 7 shows a random sample of the comparisons between the predicted and observed 20-minute surface drift segments for two sub-regions. Fig. 8 shows the final error distribution derived from this comparison; the mean error in current magnitude is 0.35 m s^{-1} (less than 0.7 m s^{-1} at the 90% confidence level). The direction is in error by 8° on average for currents over 0.7 m s^{-1} (but much larger during slack currents), and 15° at the 90% confidence level. In addition to the method and the simplifications used to produce the Atlas, the stratification, internal wave properties, sub-grid scale processes, weather (including local and remote storm surges), and precipitation events can also explain large differences between the Atlas's predictions and the real world.

In summary, the new Surface Current Atlas of the St. Lawrence Estuary was made possible through the use of new high-resolution numerical modeling and satellite geodesy. It is an update of the first atlas published in 1939, which documented local maximum flood and ebb surface current measurements.[16] Modeling permitted us to account for complex density and topographic effects and to make use of historical current-meter information. Direct surface current measurements allowed for the independent analysis of this approach. At the present time, over 1500 Atlases have been sold, and the validation continues as users report their observations against the Atlas's predictions.

Acknowledgements. Funding was provided by St. Lawrence Vision 2000. We thank Bill Crawford for his review of the Atlas and Jean Piuze and Denis Hains for their continuous support during its production.

References

1. Government of Canada, *Atlas of tidal currents: St. Lawrence Estuary from Cap de Bon-Désir to Trois-Rivières*, Dept. Fisheries and Oceans, Canadian Hydrographic Service, Ottawa, 108 + XX p., 1997.
2. Neu, H.J.A., A study on mixing and circulation in the St. Lawrence Estuary up to 1964, *Atlantic Oceano. Lab. Bed. Inst. Rep. Ser. No. 1970-9,* 31 p., 1970.
3. Backhaus, J.O., A three-dimensional model for the simulation of shelf-sea dynamics. *Dt. Hydrogr. Z.,* **38**, pp. 165-187, 1985.
4. Stronach, J.A., Backhaus, J.O. & Murty, T.S., An update on the numerical simulation of oceanographic processes in the waters between Vancouver Island and the mainland: the GF8 model, *Oceanogr. Mar. Biol. Annu. Rev.,* **31**, pp. 1-86, 1993.
5. Saucier, F.J. & Chassé, J., Tidal action on buoyancy effects in the St. Lawrence Estuary, submitted, 1998.
6. Smagorinsky, J., General circulation experiments with primitive equations. I. The basic experiment, *Monthly Weather Rev.,* **91(3)**, pp. 99-164, 1963.
7. Mellor, G.L. & Yamada, T., Development of a turbulence closure model for geophysical fluid problems, *Rev. Geophys. Space Phys.,* **20 (4)**, pp. 851-875, 1982.
8. Davies, A.M., Jones, J.E. & Xing, J., Review of recent developments in tidal hydrodynamic modeling. 2: Turbulence energy models, *J. Hydraul. Eng.* **123(4)**, pp. 293-302, 1997.
9. Mellor, G.L. & Durbin, P.A., The structure and dynamics of the ocean surface mixed layer, *J. Phys. Oceanogr.* **5**, pp. 718-728, 1975.
10. Chow, V.T., *Open channel hydraulics*, McGraw-Hill, New York, 680 p., 1959.
11. Forrester, W.D., Internal tides in the St. Lawrence Estuary. *J. Mar. Res.* **32**, pp. 55-66, 1974.
12. Foreman, M.G., Manual for tidal height analysis and prediction, *Pacific Marine Science Report No. 77-10,* Institute of Ocean Sciences, 101 p., 1977.
13. Government of Canada, *Canadian Tide and Current Tables, Vol.3*, Dept. Fisheries and Oceans, Ottawa, published yearly.
14. Dominion of Canada. *St. Lawrence River, below Quebec - Currents in the estuary, Orleans Island to the Saguenay region*, Notice to Mariners, No. 30, Atlantic No. 14, Dept. Fisheries and Oceans, Ottawa, 1936.
15. Farmer, D.M. & Freeland, H.J. The physical oceanography of fjords, *Prog. Oceanogr.,* **12**, 147-220, 1982.
16. Government of Canada, *Tidal current charts of the St. Lawrence*, Dept. Fisheries and Oceans, Canadian Hydrographic Service, Tidal publication No. 21, Ottawa, 1939.